Double-Delta Sourced Winding for Dual Winding Induction Machine

Yongsoon Park, Jeong-Mock Yoo, and Seung-Ki Sul

Department of Electrical and Computer Engineering, Seoul National University, Seoul, Korea

sulsk@plaza.snu.ac.kr

***Abstract*—The harmonic distortions of motor currents can be mitigated by the application of the double-delta sourced winding (DDSW), which implements multi-level operation with two-level converters. In practice, dual winding induction machine (DWIM) has been considered for this application due to its inherent compatibility to DDSW. The modeling of DWIM is discussed for the vector control, and a decoupling control method of each winding to the other is proposed to improve the dynamic response of the current regulation. The torque control is also discussed for the case where one of the converters is dropped out. The effectiveness of the proposed methods is assessed with experimental results. It has been confirmed that the total harmonic distortion of the converter currents was decreased by 67.7 % when DDSW was applied to an 11 kW DWIM. In addition, the bandwidth of the current regulation could be increased by 113.7 % thanks to the proposed decoupling control method.**

***Index Terms*—double-delta, fault, induction machine, multi-level, vector control**

I. Introduction

Double-delta sourced transformer had been proposed to mitigate ripple currents through multi-level operations [1]. This topology is based on the fact that multiple windings and converters are essential for power sharing in large power conversion systems. The principle of double-delta sourced transformer can be similarly applied to dual winding motors, which have been used for starting purpose or adapting dual voltage source. The two sets of winding of the motor can be easily transformed to double-delta sourced winding (DDSW) under the assumption of the isolated DC link of two converters driving each delta winding. It is expected to improve the efficiency of the converters by mitigating harmonic currents through DDSW.

Because the vector control is essential to drive motors in high performance [2], it has to be considered at first for the application of DDSW. As mentioned earlier, DDSW is appropriate for large power systems where multiple windings and converters are intrinsic. In the most of industrial applications, the induction machine is still dominant [3]. And, in this paper a dual winding induction machine is considered for the implementation of DDSW.

Induction machines are diversely classified by their starting methods [4], [5]. One type of them is designed to use series windings for starting and parallel windings for normal operation, so called dual voltage winding. For the application of DDSW, this dual winding induction machine (DWIM) is deemed an appropriate candidate. And DDSW can be easily implemented by appropriate connection of 6 terminals of stator winding of DWIM. Then, the conventional modeling can be referred for the vector control of the DDSW-applied DWIM [6], [7].

However, the stator windings are mainly assumed as wye-connected one in the literature whereas they must be delta-connected for DDSW. Hence, by considering the delta connection, the electrical modeling of DWIM is newly derived with respect to the converter currents rather than the winding currents. Accordingly, torque, flux, and slip equations are detailed for the vector control of DWIM for DDSW. In addition, the decoupling between the converters should be discussed for the current regulation since each winding of DDSW connected to one converter is simultaneously affected by the other converter. In this paper, a novel decoupling method is induced by rearranging the voltage equation of DWIM.

Meanwhile, in DDSW if one of the converters is dropped out by any reason, it would be desirable to keep the other converter working for the continuous drives. Thus, the different modeling is derived under this single converter operation for the vector control. Even if the remaining converter solely deals with the series windings, it can operate with the same DC-link voltage up to the current limit of the remaining converter. The harmonic property of the currents under this single converter operation with DDSW is also delineated.

All the proposed methods are evaluated with a small-scale induction machine, which is a commercially available product designed for dual source voltage, namely, 220V/440V. Through experimental results, the characteristics of DDSW are evidently confirmed at winding voltages and converter currents, and it is also examined whether the torque is regulated as intended. In addition, the performance of the decoupling method is conspicuously presented when torque command varies in step manner.

II. Double-Delta Sourced Winding

In Fig. 1 the direction of current of each winding of DDSW is depicted. Namely, the three-phase outputs from the converters are respectively denoted by ‘abc’ and ‘rst’ nodes, and the windings where the same back electromotive force (EMF) appears are separated by Greek alphabets. Then, it is inferred that all the winding voltages are determined by both of the converters. In other words, the pulse-width modulation (PWM) of one converter affects every winding voltage. Therefore, the

harmonic distortions of the winding currents could be improved by the appropriate simultaneous PWM of both converters.

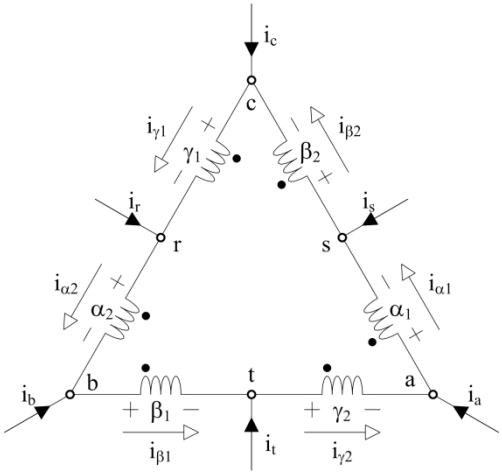

Fig. 1. Windings and currents in DDSW.

The effect of DDSW to voltage and current of each winding can be clearly demonstrated by contrasting the voltage and current waveforms of the conventional winding in Figs. 2 and 4 and those of DDSW in Fig.3 and 5. To begin with, the winding voltages on α_1 are shown in Figs. 2 and 3 where only the winding structure is different for an 11 kW DWIM with no load torque at the rated speed. By the comparison between the figures, it is easily recognized that the number of the voltage level is increased by DDSW as in the literature for the transformer [1]. Contrary to DDSW, the phase difference between the carriers of each converter for PWM, which is 180 ° in the figure, does not lead to any meaningful change of the winding voltage in the conventional structure. The property of the winding voltages is straightly reflected into the converter currents as shown in Figs. 4 and 5. While the fundamental currents are around 12.6 A for both figures, the total harmonic distortion (THD) of the current is decreased by 67.7 %, from 31.5 % to 10.2 %, by means of DDSW. Although the phase of the ripple currents is certainly opposite between the converters with conventional winding in Fig. 4, this PWM carrier shift by 180 ° is not helpful at the stator side when compared to Fig. 5.

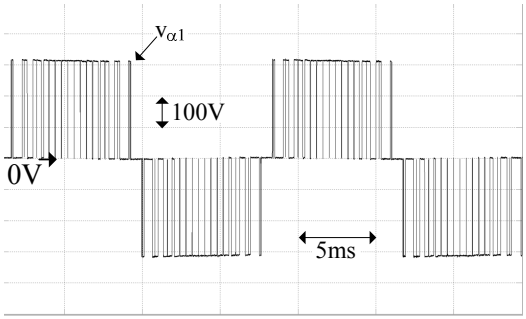

Fig. 2. Winding voltage in conventional structure.

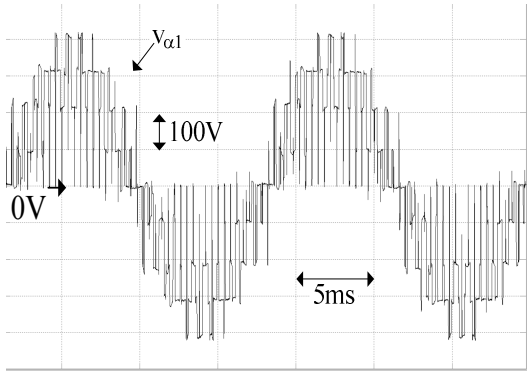

Fig. 3. Winding voltage in DDSW.

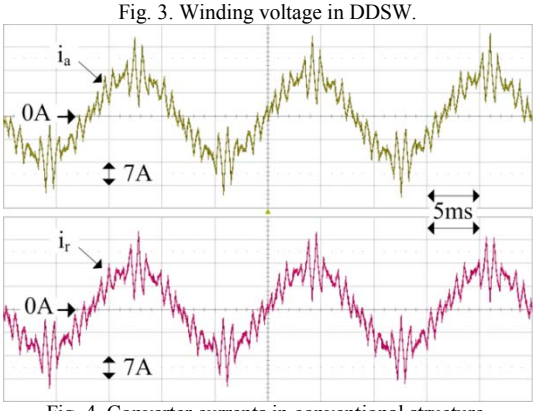

Fig. 4. Converter currents in conventional structure.

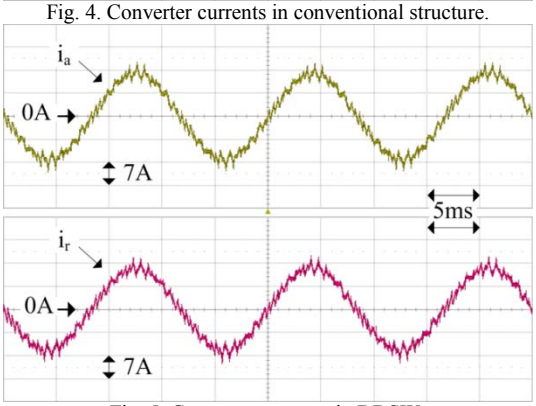

Fig. 5. Converter currents in DDSW.

The back EMFs induced on α_1, β_1, and γ_1 are expected to be the same with those on α_2, β_2, and γ_2, respectively. In other words, two set of the three-phase windings are identical in their influences to the rotating flux. Then, the equivalent two-pole machine can be modeled as shown in Fig. 6. Because this machine does not correspond to the case of split phase belt [8], [9], the mutual coupling between the leakage inductances could be neglected.

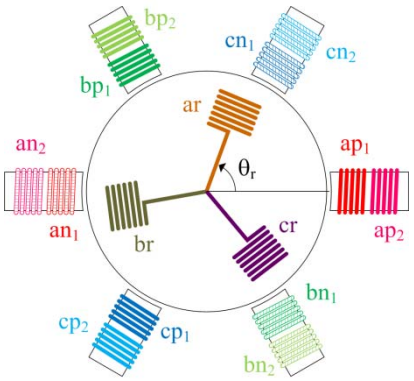

Fig. 6. Conceptual winding structure of two-pole DWIM for DDSW.

III. Modeling of DWIM for DDSW

It is assumed that the DWIM modelled has the same voltage rating for each winding. And, the rated voltage of DWIM in series connection would be two times of that in parallel connection. For example, in Fig. 6, the windings of ap_1 and ap_2 are series-connected for 440 V while parallel-connected for 220 V. Although the winding currents of ap_1 and ap_2 are identical in the conventional parallel and series modes, they can be differently regulated in DDSW.

The magnetic couplings among the stator and the rotor windings are derived as (1) by the same principle of the literature [2].

$$\begin{bmatrix}\lambda_{\alpha1}\\ \lambda_{\beta1}\\ \lambda_{\gamma1}\end{bmatrix} = L_{ls}\begin{bmatrix}i_{\alpha1}\\ i_{\beta1}\\ i_{\gamma1}\end{bmatrix} + L_{ms}A_m\begin{bmatrix}i_{\alpha1}+i_{\alpha2}\\ i_{\beta1}+i_{\beta2}\\ i_{\gamma1}+i_{\gamma2}\end{bmatrix} + L_{ms}T_{rs}\begin{bmatrix}i_{ar}\\ i_{br}\\ i_{cr}\end{bmatrix} \quad (1\text{-a})$$

$$\begin{bmatrix}\lambda_{\alpha2}\\ \lambda_{\beta2}\\ \lambda_{\gamma2}\end{bmatrix} = L_{ls}\begin{bmatrix}i_{\alpha2}\\ i_{\beta2}\\ i_{\gamma2}\end{bmatrix} + L_{ms}A_m\begin{bmatrix}i_{\alpha1}+i_{\alpha2}\\ i_{\beta1}+i_{\beta2}\\ i_{\gamma1}+i_{\gamma2}\end{bmatrix} + L_{ms}T_{rs}\begin{bmatrix}i_{ar}\\ i_{br}\\ i_{cr}\end{bmatrix} \quad (1\text{-b})$$

$$\begin{bmatrix}\lambda_{ar}\\ \lambda_{br}\\ \lambda_{cr}\end{bmatrix} = (L_{lr}+L_{ms}A_m)\begin{bmatrix}i_{ar}\\ i_{br}\\ i_{cr}\end{bmatrix} + L_{ms}T_{sr}\begin{bmatrix}i_{\alpha1}+i_{\alpha2}\\ i_{\beta1}+i_{\beta2}\\ i_{\gamma1}+i_{\gamma2}\end{bmatrix} \quad (1\text{-c})$$

,where L_{ls} and L_{lr} are the leakage inductances of the stator and rotor windings, respectively. In addition, L_{ms} is the mutual inductance. The unexplained matrices in (1) are shown in

$$A_m = \begin{bmatrix}1 & -1/2 & -1/2\\ -1/2 & 1 & -1/2\\ -1/2 & -1/2 & 1\end{bmatrix} \quad (2\text{-a})$$

$$T_{rs} = \begin{bmatrix}\cos\theta_r & \cos(\theta_r+\frac{2\pi}{3}) & \cos(\theta_r-\frac{2\pi}{3})\\ \cos(\theta_r-\frac{2\pi}{3}) & \cos\theta_r & \cos(\theta_r+\frac{2\pi}{3})\\ \cos(\theta_r+\frac{2\pi}{3}) & \cos(\theta_r-\frac{2\pi}{3}) & \cos\theta_r\end{bmatrix} \quad (2\text{-b})$$

$$T_{sr} = \begin{bmatrix}\cos\theta_r & \cos(\theta_r-\frac{2\pi}{3}) & \cos(\theta_r+\frac{2\pi}{3})\\ \cos(\theta_r+\frac{2\pi}{3}) & \cos\theta_r & \cos(\theta_r-\frac{2\pi}{3})\\ \cos(\theta_r-\frac{2\pi}{3}) & \cos(\theta_r+\frac{2\pi}{3}) & \cos\theta_r\end{bmatrix} \quad (2\text{-c})$$

, where θ_r is the rotor angle and is defined in Fig. 6.

The flux equation in (1) is pertaining to the winding currents. However, it is more practical to consider the currents of the converters than the windings since current sensors for the current regulation are commonly installed in the converters. Equation (3) is derived from Fig. 1 by Kirchhoff's current law (KCL).

$$\begin{cases} i_a = i_{\alpha1} - i_{\gamma2}\\ i_b = i_{\beta1} - i_{\alpha2}\\ i_c = i_{\gamma1} - i_{\beta2}\end{cases} \quad (3\text{-a})$$

$$\begin{cases} i_r = i_{\alpha2} - i_{\gamma1}\\ i_s = i_{\beta2} - i_{\alpha1}\\ i_t = i_{\gamma2} - i_{\beta1}\end{cases}. \quad (3\text{-b})$$

When considering (3), equation (1) can be rearranged into (4) by the subtractions between the fluxes.

$$\begin{bmatrix}\lambda_a\\ \lambda_b\\ \lambda_c\end{bmatrix} = L_{ls}\begin{bmatrix}i_a\\ i_b\\ i_c\end{bmatrix} + \frac{3}{2}L_{ms}\begin{bmatrix}i_a+i_r\\ i_b+i_s\\ i_c+i_t\end{bmatrix} + L_{ms}T_{rs}\begin{bmatrix}i_u\\ i_v\\ i_w\end{bmatrix} \quad (4\text{-a})$$

$$\begin{bmatrix}\lambda_r\\ \lambda_s\\ \lambda_t\end{bmatrix} = L_{ls}\begin{bmatrix}i_r\\ i_s\\ i_t\end{bmatrix} + \frac{3}{2}L_{ms}\begin{bmatrix}i_a+i_r\\ i_b+i_s\\ i_c+i_t\end{bmatrix} + L_{ms}T_{rs}\begin{bmatrix}i_u\\ i_v\\ i_w\end{bmatrix} \quad (4\text{-b})$$

$$\begin{bmatrix}\lambda_u\\ \lambda_v\\ \lambda_w\end{bmatrix} = (L_{lr}+\frac{3}{2}L_{ms})\begin{bmatrix}i_u\\ i_v\\ i_w\end{bmatrix} + L_{ms}T_{sr}\begin{bmatrix}i_a+i_r\\ i_b+i_s\\ i_c+i_t\end{bmatrix} \quad (4\text{-c})$$

$$\begin{bmatrix}i_u\\ i_v\\ i_w\end{bmatrix} = \begin{bmatrix}i_{ar}-i_{cr}\\ i_{br}-i_{ar}\\ i_{cr}-i_{br}\end{bmatrix}. \quad (5)$$

The rotor currents can be derived in (5) through the subtractions by themselves to maintain the consistency between (1) and (4). That is, (4) can be regarded as a fictitious model of DWIM for control. In terms of the converter currents, the voltage equation of the DDSW would be completely derived if the resistance drop is added to the time differential of (4). Initially, the winding voltages are expressed with the converter voltages as (6) by the superposition principle [1].

$$\begin{cases} v_{\alpha1} = v_{ae} - v_{se}\\ v_{\beta1} = v_{be} - v_{te}\\ v_{\gamma1} = v_{ce} - v_{re}\end{cases} \quad (6\text{-a})$$

$$\begin{cases} v_{\alpha2} = v_{re} - v_{be}\\ v_{\beta2} = v_{se} - v_{ce}\\ v_{\gamma2} = v_{te} - v_{ae}\end{cases} \quad (6\text{-b})$$

, where the subscript 'e' means the effective converter voltage without common mode components, and the sum of three-phase effective voltage is null.

As the flux equation in (4), the voltage equation can be derived as (7) through subtractions.

$$\begin{bmatrix} v_{af} \\ v_{bf} \\ v_{cf} \end{bmatrix} = \begin{bmatrix} v_{\alpha 1} - v_{\gamma 2} \\ v_{\beta 1} - v_{\alpha 2} \\ v_{\gamma 1} - v_{\beta 2} \end{bmatrix} = R_s \begin{bmatrix} i_a \\ i_b \\ i_c \end{bmatrix} + \frac{d}{dt} \begin{bmatrix} \lambda_a \\ \lambda_b \\ \lambda_c \end{bmatrix} = \begin{bmatrix} 2v_{ae} + v_{re} \\ 2v_{be} + v_{se} \\ 2v_{ce} + v_{te} \end{bmatrix} \quad (7\text{-a})$$

$$\begin{bmatrix} v_{rf} \\ v_{sf} \\ v_{tf} \end{bmatrix} = \begin{bmatrix} v_{\alpha 2} - v_{\gamma 1} \\ v_{\beta 2} - v_{\alpha 1} \\ v_{\gamma 2} - v_{\beta 1} \end{bmatrix} = R_s \begin{bmatrix} i_r \\ i_s \\ i_t \end{bmatrix} + \frac{d}{dt} \begin{bmatrix} \lambda_r \\ \lambda_s \\ \lambda_t \end{bmatrix} = \begin{bmatrix} 2v_{re} + v_{ae} \\ 2v_{se} + v_{be} \\ 2v_{te} + v_{ce} \end{bmatrix} \quad (7\text{-b})$$

$$\begin{bmatrix} v_u \\ v_v \\ v_w \end{bmatrix} = \begin{bmatrix} v_{ar} - v_{cr} \\ v_{br} - v_{ar} \\ v_{cr} - v_{br} \end{bmatrix} = R_r \begin{bmatrix} i_u \\ i_v \\ i_w \end{bmatrix} + \frac{d}{dt} \begin{bmatrix} \lambda_u \\ \lambda_v \\ \lambda_w \end{bmatrix} \quad (7\text{-c})$$

, where R_s and R_r are stator and rotor winding resistances, respectively.

By using the concept of the complex space vector [2], the three-phase variables in (4) and (7) are presented as rotating vectors in a plane. In addition, these complex vectors can be considered in the rotating reference frame, which rotates with an arbitrary rotating frequency, ω. Then, (8) is obtained from (4) while (9) from (7).

$$\vec{\lambda}_{dqs1} = L_s \vec{i}_{dqs1} + L_m (\vec{i}_{dqs2} + \vec{i}_{dqr}) \quad (8\text{-a})$$

$$\vec{\lambda}_{dqs2} = L_s \vec{i}_{dqs2} + L_m (\vec{i}_{dqs1} + \vec{i}_{dqr}) \quad (8\text{-b})$$

$$\vec{\lambda}_{dqr} = L_r \vec{i}_{dqr} + L_m (\vec{i}_{dqs1} + \vec{i}_{dqs2}) \quad (8\text{-c})$$

$$\vec{v}_{dqs1} = R_s \vec{i}_{dqs1} + \frac{d}{dt} \vec{\lambda}_{dqs1} + j\omega \cdot \vec{\lambda}_{dqs1} \quad (9\text{-a})$$

$$\vec{v}_{dqs2} = R_s \vec{i}_{dqs2} + \frac{d}{dt} \vec{\lambda}_{dqs2} + j\omega \cdot \vec{\lambda}_{dqs2} \quad (9\text{-b})$$

$$\vec{v}_{dqr} = R_r \vec{i}_{dqr} + \frac{d}{dt} \vec{\lambda}_{dqr} + j(\omega - \omega_r) \cdot \vec{\lambda}_{dqr} \quad (9\text{-c})$$

where L_m is equal to $1.5 \cdot L_{ms}$. In addition, L_s is the sum of L_{ls} and L_m while L_r is the sum of L_{lr} and L_m.

In the basis of (9), the equivalent circuit of DWIM with DDSW is drawn as Fig. 7 in the synchronously rotating reference frame, which is identical to those of DWIM in the literature [6]. However, the ratings of currents, voltages, and fluxes need to be further addressed for DDSW.

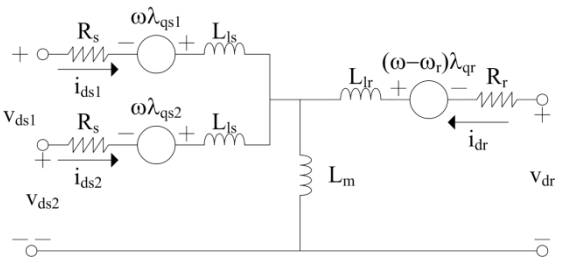

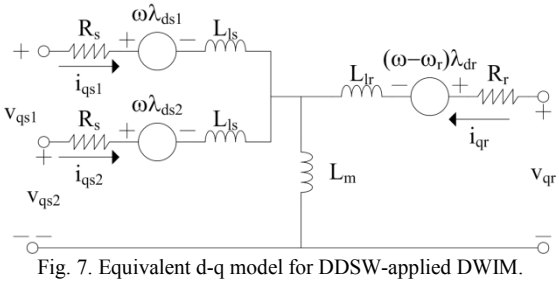

Fig. 7. Equivalent d-q model for DDSW-applied DWIM.

As well known for normal induction machines, the d-axis rotor flux and the slip frequency are respectively derived as (10) and (11) from (9) if ω in (9) is set such that the q-axis rotor flux is null.

$$\lambda_{dr} = \frac{L_m}{1 + s \cdot L_r / R_r} (i_{ds1} + i_{ds2}) \quad (10)$$

$$\omega_{sl} = \omega - \omega_r = \frac{R_r}{L_r} \frac{L_m}{\lambda_{dr}} (i_{qs1} + i_{qs2}) \quad (11)$$

where 's' indicates the Laplace operator.

When it comes to the rotor flux and the slip frequency, it is not difficult to prove that the same formulas can be derived with respect to converter current even if the equivalent model is induced with respect to the winding currents. However, the magnitude of converter currents is $\sqrt{3}$ times that of the winding currents when considering (3). Then, the rated rotor flux in the converter-based model is $\sqrt{3}$ times that in the winding-based model. This has to be recognized as a scale difference between the modeling methods. As mentioned earlier, the fictitious plant was assumed to express the flux and voltage equations in the view point of the converter current and voltage.

The scale difference seems to be observed for the slip frequency in (11) due to the q-axis currents. However, because the rotor flux in the denominator offset the scale difference of the q-axis currents, the slip frequency has the same magnitude in both of the winding-based and the converter-based models.

In addition, the torque equation can be derived from the power equation, where the products of voltages and currents in (9) are summed. Namely, the electrical power of DWIM, P_e, can be expressed with

$$P_e = \eta_m \cdot Re[\vec{v}_{dqs1} \cdot \vec{i}^{*}_{dqs1} + \vec{v}_{dqs2} \cdot \vec{i}^{*}_{dqs2} + \vec{v}_{dqr} \cdot \vec{i}^{*}_{dqr}] \quad (12)$$

where the asterisk '*' represents complex conjugate, and η_m is introduced for scaling.

After eliminating copper losses and the varying energy of inductances [2], the component related to torque can be separated. In conclusion, the torque equation can be derived as

$$T_e = \frac{1}{2} \frac{P}{2} \frac{L_m}{L_r} \cdot \lambda_{dr} (i_{qs1} + i_{qs2}) . \quad (13)$$

Because both of the rotor flux and the q-axis current in the converter-based model are $\sqrt{3}$ times those in the winding-based model, η_m must be 1/2 to consistently maintain the same dimension for power.

As widely known [2], the vector control of DWIM with DDSW can also be achieved by adjusting the d-q

currents when considering (10) and (13). Namely, the d-axis currents are effective to modulate the rotor flux while the q-axis currents to modulate the torque. In addition, the synchronous frequency can be obtained from the sum of the slip frequency by (11) and the rotating frequency, ω_r.

IV. Decoupling Method for Current Regulation

The current regulation on the converter currents is essential since the torque and flux are modulated by the currents. However, from (7), it is evident that the currents of each converter are affected by both of the converters. Moreover, they are also coupled through flux as shown in (4). These interferences between the converters should be decoupled for better dynamics of DWIM.

Initially, the voltage coupling can be prevented by the matrix operation in (7). For example, the abc-current is influenced by both of the effective converter voltages. However, from the same equation, it is inferred that this current is only altered by v_{af}, v_{bf}, and v_{cf}, not by v_{rf}, v_{sf}, and v_{tf}. If the current regulators are designed with respect to these imaginary three-phase voltages, its performance is not disturbed as if the voltage coupling disappears. Instead, the conversion from the imaginary voltage to the converter voltage has to be added as shown in (14).

$$\begin{bmatrix} v_{d1} \\ v_{d2} \\ v_{q1} \\ v_{q2} \end{bmatrix} = \frac{1}{3}\begin{bmatrix} 2 & -1 & 0 & 0 \\ -1 & 2 & 0 & 0 \\ 0 & 0 & 2 & -1 \\ 0 & 0 & -1 & 2 \end{bmatrix}\begin{bmatrix} v_{ds1} \\ v_{ds2} \\ v_{qs1} \\ v_{qs2} \end{bmatrix} \tag{14}$$

where v_{d1}, v_{q1}, v_{d2}, and v_{q2} are the d-q voltages of the effective converter voltages. Equation (14) comes from (7).

In order to eliminate the flux coupling, the voltage equation needs to be rearranged from (9) to (15) without the rotor currents, which are deemed uncontrollable variables in squirrel-cage induction machines [7].

$$\vec{v}_{dqs1} = (R_s + \frac{R_r L_m^2}{L_r^2})\vec{i}_{dqs1} + L_{ss}\frac{d}{dt}\vec{i}_{dqs1} + L_{sc}\frac{d}{dt}\vec{i}_{dqs2} + \frac{R_r L_m^2}{L_r^2}\vec{i}_{dqs2} + j\omega L_{ls}\vec{i}_{dqs1} + \vec{v}_{comm} \tag{15-a}$$

$$\vec{v}_{dqs2} = (R_s + \frac{R_r L_m^2}{L_r^2})\vec{i}_{dqs2} + L_{ss}\frac{d}{dt}\vec{i}_{dqs2} + L_{sc}\frac{d}{dt}\vec{i}_{dqs1} + \frac{R_r L_m^2}{L_r^2}\vec{i}_{dqs1} + j\omega L_{ls}\vec{i}_{dqs2} + \vec{v}_{comm} \tag{15-b}$$

$$L_{sc} = L_m - L_m^2/L_r \tag{15-c}$$

$$L_{ss} = L_s - L_m^2/L_r = L_{ls} + L_{sc} \tag{15-d}$$

$$\vec{v}_{comm} = \frac{L_m}{L_r}(-\frac{R_r}{L_r} + j\omega_r)\cdot\vec{\lambda}_{dqr} + j\omega L_{sc}(\vec{i}_{dqs1} + \vec{i}_{dqs2}). \tag{15-e}$$

Due to the flux coupling, there are the cross coupled differential terms in (15-a) and (15-b). In the literature, this differential cross-coupling was ignored, and the speed-related terms were only used for the feed-forward control in addition to the output of the proportional and integral (PI) controllers as shown in Fig. 8 [7]. For the decoupling control, (15) can be rearranged into (16).

$$\begin{bmatrix} L_{ss} & L_{sc} \\ L_{sc} & L_{ss} \end{bmatrix}\cdot\frac{d}{dt}\begin{bmatrix} \vec{i}_{dqs1} \\ \vec{i}_{dqs2} \end{bmatrix} = \begin{bmatrix} \vec{v}_{dqs1} \\ \vec{v}_{dqs2} \end{bmatrix} - \begin{bmatrix} (R_s + \frac{R_r L_m^2}{L_r^2})\vec{i}_{dqs1} + \frac{R_r L_m^2}{L_r^2}\vec{i}_{dqs2} + j\omega L_{ls}\vec{i}_{dqs1} + \vec{v}_{comm} \\ (R_s + \frac{R_r L_m^2}{L_r^2})\vec{i}_{dqs2} + \frac{R_r L_m^2}{L_r^2}\vec{i}_{dqs1} + j\omega L_{ls}\vec{i}_{dqs2} + \vec{v}_{comm} \end{bmatrix}. \tag{16}$$

From (16), the voltage equation can be derived as (17).

$$\begin{bmatrix} \vec{v}_{dqe1} \\ \vec{v}_{dqe2} \end{bmatrix} = R_{ss}\begin{bmatrix} \vec{i}_{dqs1} \\ \vec{i}_{dqs2} \end{bmatrix} + L_{se}\frac{d}{dt}\begin{bmatrix} \vec{i}_{dqs1} \\ \vec{i}_{dqs2} \end{bmatrix} + \begin{bmatrix} R_{sc}\vec{i}_{dqs2} + j\omega(L_{ss}\vec{i}_{dqs1} - L_{sc}\vec{i}_{dqs2}) + \vec{v}_{comm} \\ R_{sc}\vec{i}_{dqs1} + j\omega(L_{ss}\vec{i}_{dqs2} - L_{sc}\vec{i}_{dqs1}) + \vec{v}_{comm} \end{bmatrix} \tag{17-a}$$

$$\begin{bmatrix} \vec{v}_{dqs1} \\ \vec{v}_{dqs2} \end{bmatrix} = \frac{1}{L_{se}}\begin{bmatrix} L_{ss} & L_{sc} \\ L_{sc} & L_{ss} \end{bmatrix}\begin{bmatrix} \vec{v}_{dqe1} \\ \vec{v}_{dqe2} \end{bmatrix} \tag{17-b}$$

$$R_{ss} = \frac{R_s L_{ss}}{L_{ls}} + \frac{R_r L_m^2}{L_r^2} \tag{17-c}$$

$$R_{sc} = \frac{R_r L_m^2}{L_r^2} - \frac{R_s L_{sc}}{L_{ls}} \tag{17-d}$$

$$L_{se} = L_{ss} + L_{sc}. \tag{17-e}$$

The differential cross-coupling is not seen any more in (17) by virtue of the additional linear algebra. Instead, like (14), the calculation of converter voltage by (17-b) is required for the decoupling.

If the feed-forward compensation is perfect ($\hat{v}_{ff} = v_{ff}$), the dynamic response of the current regulation can be expressed with (18) by setting the PI gains according to (19).

$$\frac{i}{i^*} = \frac{\omega_c}{s + \omega_c} \tag{18}$$

$$k_p = L\omega_c,\ k_i = R\omega_c \tag{19}$$

where ω_c is the bandwidth of the current regulator.

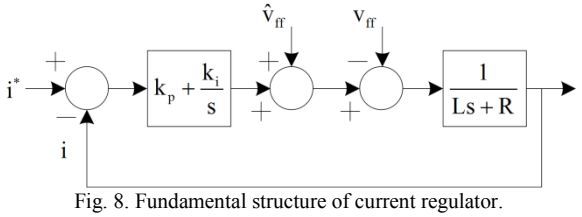

Fig. 8. Fundamental structure of current regulator.

For the current regulation of DWIM, R_{ss} and L_{se} in (17) correspond to R and L in Fig. 8, respectively. Except them, the rest of terms in the right-side of (17-a) is used for the feed-forward voltage.

V. Single Converter Operation in DDSW-Applied DWIM

Two converters are necessary to construct DDSW in Fig. 1. However, one of them might be dropped out by any reason such as fault in a converter. In preparation for this disconnection, single converter operation mode needs

to be considered for the continuous drives of DWIM with DDSW. If the one converter, namely 'rst' converter is disconnected in Fig. 1, the voltage equation can be derived as (20) by the series connection of windings.

$$\begin{bmatrix} 3v_{ae} \\ 3v_{be} \\ 3v_{ce} \end{bmatrix} = 2R_s \begin{bmatrix} i_a \\ i_b \\ i_c \end{bmatrix} + \frac{d}{dt} \begin{bmatrix} \lambda_{\alpha 1} + \lambda_{\beta 2} - \lambda_{\beta 1} - \lambda_{\gamma 2} \\ \lambda_{\beta 1} + \lambda_{\gamma 2} - \lambda_{\gamma 1} - \lambda_{\alpha 2} \\ \lambda_{\gamma 1} + \lambda_{\alpha 2} - \lambda_{\alpha 1} - \lambda_{\beta 2} \end{bmatrix} \cdot \quad (20)$$
$$= 2R_s \begin{bmatrix} i_a \\ i_b \\ i_c \end{bmatrix} + \frac{d}{dt} \begin{bmatrix} \lambda_a \\ \lambda_b \\ \lambda_c \end{bmatrix}$$

In fact, the 'abc' flux in (20) is different from that in (4), and can be detailed with (21).

$$\begin{bmatrix} \lambda_a \\ \lambda_b \\ \lambda_c \end{bmatrix} = (2L_{ls} + \frac{3}{2} L_{ms}) \begin{bmatrix} i_a \\ i_b \\ i_c \end{bmatrix} + L_{ms} T_{rsf} \begin{bmatrix} i_x \\ i_y \\ i_z \end{bmatrix} \quad (21\text{-a})$$

$$\begin{bmatrix} i_x \\ i_y \\ i_z \end{bmatrix} = \begin{bmatrix} i_{ar} - i_{br} \\ i_{br} - i_{cr} \\ i_{cr} - i_{ar} \end{bmatrix} \quad (21\text{-b})$$

$$T_{rsf} = \begin{bmatrix} \cos(\theta_r - \frac{\pi}{3}) & \cos(\theta_r + \frac{\pi}{3}) & \cos(\theta_r + \pi) \\ \cos(\theta_r + \pi) & \cos(\theta_r - \frac{\pi}{3}) & \cos(\theta_r + \frac{\pi}{3}) \\ \cos(\theta_r + \frac{\pi}{3}) & \cos(\theta_r + \pi) & \cos(\theta_r - \frac{\pi}{3}) \end{bmatrix}. \quad (21\text{-c})$$

Moreover, since the subtractions between the rotor currents in (21-b) are also different to those in (5), the rotor flux equation is newly derived as (22).

$$\begin{bmatrix} \lambda_x \\ \lambda_y \\ \lambda_z \end{bmatrix} = \begin{bmatrix} \lambda_{ar} - \lambda_{br} \\ \lambda_{br} - \lambda_{cr} \\ \lambda_{cr} - \lambda_{ar} \end{bmatrix} = (L_{lr} + \frac{3}{2} L_{ms}) \begin{bmatrix} i_x \\ i_y \\ i_z \end{bmatrix} + L_{ms} T_{srf} \begin{bmatrix} i_a \\ i_b \\ i_c \end{bmatrix} \quad (22\text{-a})$$

$$T_{srf}[\theta_r] = \begin{bmatrix} \cos(\theta_r - \frac{\pi}{3}) & \cos(\theta_r + \pi) & \cos(\theta_r + \frac{\pi}{3}) \\ \cos(\theta_r + \frac{\pi}{3}) & \cos(\theta_r - \frac{\pi}{3}) & \cos(\theta_r + \pi) \\ \cos(\theta_r + \pi) & \cos(\theta_r + \frac{\pi}{3}) & \cos(\theta_r - \frac{\pi}{3}) \end{bmatrix}. \quad (22\text{-b})$$

Through the similar derivations, the rotor flux and the slip frequency can be represented as (23) and (24).

$$\lambda_{dr} = \frac{L_m}{1 + s \cdot L_r / R_r} i_{ds1} \quad (23)$$

$$\omega_{sl} = \omega - \omega_r = \frac{R_r}{L_r} \frac{L_m}{\lambda_{dr}} i_{qs1}. \quad (24)$$

When compared to (10) and (11), the currents related to the 'rst' converter are disappeared. This is also observed in the torque equation under the single converter operation.

$$T_e = \frac{1}{2} \cdot \frac{P}{2} \frac{L_m}{L_r} \cdot \lambda_{dr} \cdot i_{qs1}. \quad (25)$$

That is, if the same currents are regulated for the d-q current of the remaining converter, the torque output becomes one fourth of that in the normal operation. Since the rated excitation current, corresponding to d-axis current, is less than one third of the rated current in the large-scale induction machines, the d-axis current can be doubled to keep the excitation level of DWIM with negligible reduction of the q axis current magnitude under the current limitation. With this operation strategy under the single converter operation, the torque of DWIM can be extended to almost a half of the value in the case of dual converter operation. And, the output power of DWIM of single converter operation could be almost a half of the rated one. For the current regulation, the voltage equation in (26) is finally derived. Since there is no cross-coupling in the single converter operation mode, the current regulators are designed according to (26).

$$3\vec{v}_{dq} = 2(R_s + \frac{R_r L_m^2}{L_r^2}) \vec{i}_{dqs} + L_{sf} \frac{d}{dt} \vec{i}_{dqs} \quad (26\text{-a})$$
$$+ \frac{L_m}{L_r} (-\frac{2R_r}{L_r} + j\omega_r) \cdot \vec{\lambda}_{dqr} + j\omega L_{sf} \vec{i}_{dqs}$$

$$L_{sf} = L_{ss} + L_{ls}. \quad (26\text{-b})$$

VI. Experimental Results

An 11 kW DWIM, namely 220V/440V in Fig. 9, was used to evaluate the proposed modeling and control methods for DWIM with DDSW. A DC machine was mechanically coupled with DWIM to generate various load conditions. The carrier frequency was set to 2.5 kHz, and the DC-links of the converters are set to 310 V. Particularly, the results shown in Figs. 2~5 have been obtained under the same carrier frequency of 1.25 kHz for fair comparison. The carrier frequency has been set to emulate multi-megawatt drives.

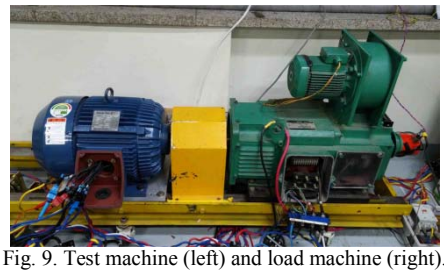

Fig. 9. Test machine (left) and load machine (right).

Initially, the torque equation in (13) was examined as shown in Fig. 10, where the test machine carried out the speed control at 1200 r/min against the load torque variation by 20 N·m. Then, the torque output by the test machine, T_{DWIM}, had to deal with friction torques and the load torque from the load machine, T_{load}. In that T_{load} was also the reference to the load machine, the error between the torque-variations of each machine could be regarded as reasonable. The d-q current was presented only for the 'abc' converter because for the 'rst' converter it was almost the same. Therefore, the value of 1/2 is appropriate for η_m in (12).

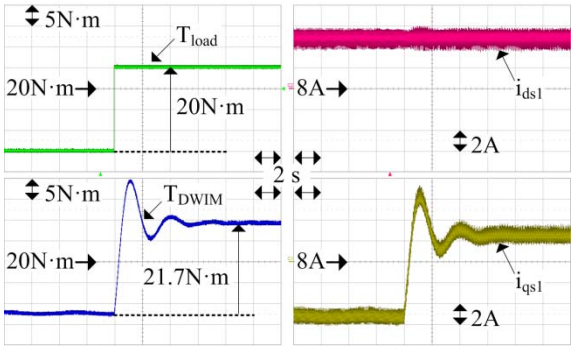

Fig. 10. Torque output under normal operation.

The major portion of high power motor drives are related to fan/pump, whose load is proportional to the square of rotating speed. Thus, the fan/pump load was emulated by using the load machine as shown in Figs. 11 and 12. Because the d-axis currents are constantly regulated as their rated value in Fig. 12, the q-axis currents are similarly changed with T_{load} of Fig. 11. The aspect of ripple currents in Fig. 12 was changed since the PWM property of DDSW varied depending on the modulation indices.

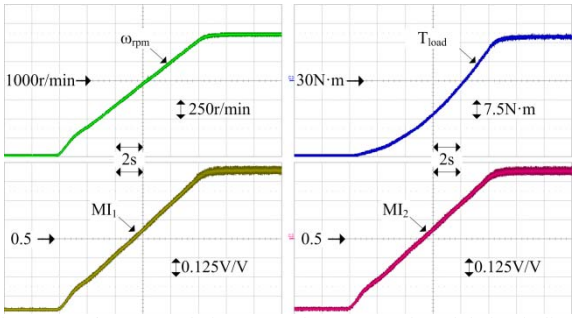

Fig. 11. Fan/pump emulation – speed, torque, and modulation indices.

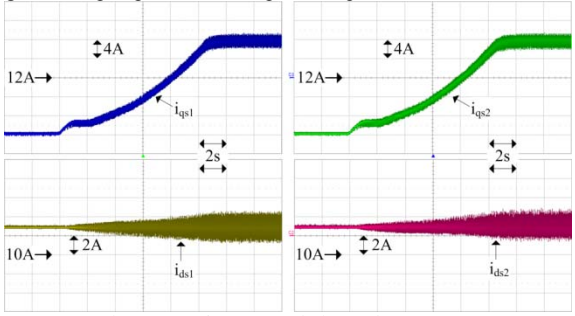

Fig. 12. Fan/pump emulation – d-q currents.

To discuss the decoupling method, the load machine was speed-controlled at 900 r/min while the test machine torque-controlled. Then, T_{DWIM} was step-changed by 30 N·m as shown in Figs. 13 and 14, where the decoupling methods were different. Because the current responses to their references were designed to follow (18), their property could be numerically addressed with their bandwidth. Namely, when the intended bandwidth was 150 Hz by using the same parameters for the gain settings, the actual bandwidth was computed as 50.2 Hz from 3τ in Fig. 13 for the conventional method whereas 107.3 Hz in Fig. 14 for the proposed decoupling method. This improvement was possible because the cross coupled differential terms were not disregarded in the proposed method. Although the bandwidth of the proposed method was smaller than the designed one, it should be reminded that nominal parameters were used for the gain settings and the feed-forward compensations would not be perfect.

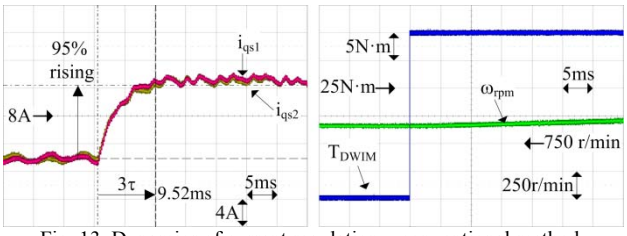

Fig. 13. Dynamics of current regulation – conventional method.

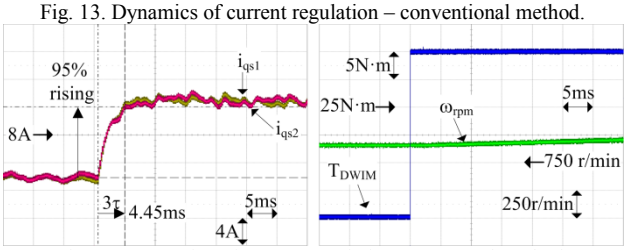

Fig. 14. Dynamics of current regulation – proposed method.

In addition, the torque equation in (25) has been examined under the single converter operation mode, where the 'rst' converter is disconnected. As the reduction of the torque per current was expected, the load torque was changed by 5 N·m at 1200 r/min as shown in Fig. 15, which was one fourth of that in Fig. 10. Then, the q-axis current was changed by 11.7 A to increase 8.2 N·m in T_{DWIM}. In other words, the torque per q-axis current was 0.7 N·m/A whereas that was 1.36 N·m/A in Fig. 10. This is because the rotor flux was halved under the single converter operation. In Fig. 16, the results with two times of d-axis current under the same load torque transient is shown, where the torque per q-axis current is two times of the q-axis current in Fig. 15. Namely, if the rotor flux is maintained to the rated value by increasing d-axis current twice under the single converter operation mode, the torque capability can be kept as a half of the value in the case of dual converter operation.

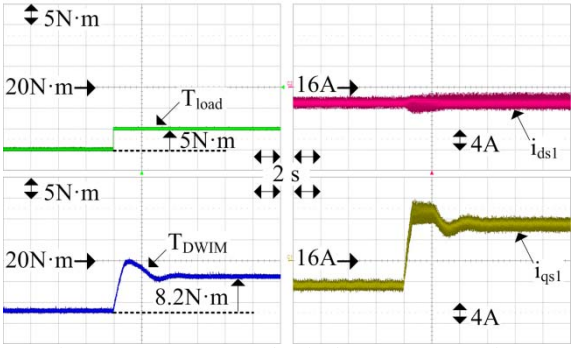

Fig. 15. Torque output under single converter operation.

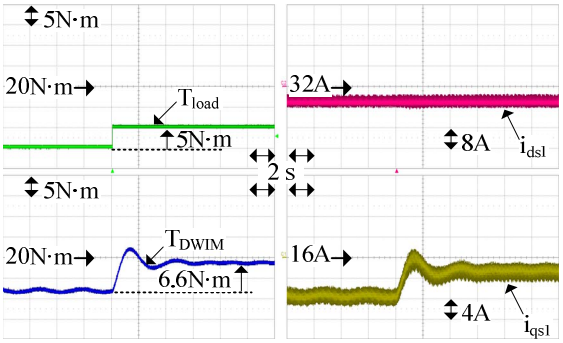

Fig. 16. Torque output under single converter operation with two times of d-axis current

In order to discuss the harmonic distortions, the converter currents are shown in Fig. 17 at the rated speed with no load torque. In addition, the carrier frequency was set to 1.25 kHz for the fair comparison to Figs. 4 and 5. In principle, it seems plausible that the harmonic distortions become worse under the single converter operation because one of the converters is dropped out in the process of the interleaving. However, as shown in Fig. 17, the THD of i_a was 11.2 % when the fundamental current was 13.5 A. That is, the harmonic property under the single converter operation is comparable to that under the normal operation of DDSW.

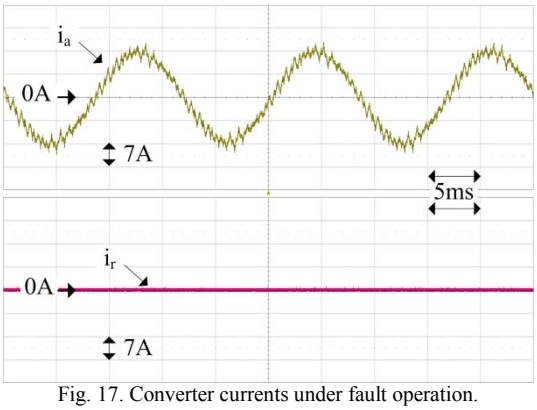

Fig. 17. Converter currents under fault operation.

.

VII. Conclusions

In this paper, the application of DDSW to DWIM has been discussed. Initially, it has been described how the vector control is implemented for DWIM with DDSW. For control purpose, the equivalent model was derived with respect to the converter currents. The feasibility of the proposed vector control was tested by emulating a fan/pump load. In addition, a decoupling method for each converter was proposed to improve the dynamic response of the current regulation. As a result, the control bandwidth could be increased by 113.7 % when the same parameters were used for control. Finally, the single converter operation has been considered, where one of the converter are disconnected from DDSW. For this operation mode, after the vector control was discussed, the harmonic properties were examined in terms of the converter current. It has been confirmed that the torque capability of DWIM with DDSW can be kept as a half of the value in the case of dual converter operation without any degradation of harmonics in the motor current.

REFERENCES

[1] Y. Park, S. Ohn, and S.-K. Sul, "Multi-Level Operation with Two-Level Converters Through a Double-Delta Source Connected Transformer," *Journal of Power Electron.*, vol. 14, no. 6, pp. 1093-1099, Nov. 2014.

[2] D. W. Novotny, and T. A. Lipo, "d,q Modeling of Induction and Synchronous Machines," *in Vector Control and Dynamics of AC Drives*, NY: Oxford Univ. Press Inc., ch. 2, pp. 35-107, 1996.

[3] S.Malik and D.Kluge, ACS1000 World's First Standard AC Drive for Medium-Voltage Applications, ABB Review, No.2, pp. 4-11, 1998..

[4] P. Vas, "Induction machine windings, starting, braking, and speed control techniques," *in Electrical Machines and Drives a space-vector theory approach*, NY: Oxford Univ. Press Inc., ch. 3.1, pp. 224-225, 1992.

[5] A. L. Sheldrake, "Methods of starting induction motors," *in Handbook of Electrical Engineering for Practitioners in the Oil, Gas, and Petrochemical Industry*, NJ: John Wiley & Sons Inc., ch. 5.10, pp. 125-129, 2003.

[6] R. H. Nelson, and P. C. Krause, "Induction Machine Analysis for Arbitrary Displacement Between Multiple Winding Sets," *IEEE Trans. Power Apparatus and Systems*, vol. PAS-93, no. 3, pp. 841-848, May 1974.

[7] R. Bojoi, F. Profumo, and A. Tenconi, "Digital Synchronous Frame Current Regulation for Dual Three-Phase Induction Motor Drives," *IEEE Power Electron. Specialist Conf. (PESC'03)*, vol. 3, pp. 1475-1480, 15-19 June 2003.

[8] T. A. Lipo, "A d-q Model for Six Phase Induction Machines," *International Conf. on Electric Machines*, 1980, pp. 860-867.

[9] O. Ojo, and I. E. Davidson, "PWM-VSI Inverter-Assisted Stand-Alone Dual Stator Winding Induction Generator," *IEEE Trans. Ind. Appl.*, vol. 36, no. 6, pp. 1604-1611, Nov./Dec. 2000.

[10] S.-K. Sul, "Design of regulators for electric machines and power converters," *in Control of Electric Machine Drive Systems*, NJ: Wiley, ch. 4, pp. 154-282, 2011.